System to Chip-level EMC/EMI Testbed Based on Miniaturized Active Optical Near-Field Time Domain Sensors

Sven Kühn[1,2], Beyhan Kochali[2], Eugen Grobbelaar[2], Niels Kuster[1,3]*

[1]Foundation for Research on Information Technologies in Society (IT'IS), 8004 Zurich, Switzerland,
kuehn@itis.ethz.ch, kuster@itis.ethz.ch

[2]Schmid & Partner Engineering AG (SPEAG), 8004 Zurich, Switzerland
wild@speag.com, eugene@speag.com, sepan@speag.com, kochali@speag.com, fuchs@speag.com, lienemann@speag.com

[3]Swiss Federal Institute of Technology (ETH) Zurich, 8092 Zurich, Switzerland

Abstract

We present an automated near-field testbed for system- to chip-level EMC/EMI evaluations in the RF domain. The scanning system combines a large scanning volume of 500 × 500 × 100 mm^3 with micrometer resolution. A novel optical surface reconstruction system allows measurement of the geometrical structure of the device under test (DUT) with better than 20μm uncertainty. This allows scanning at a precise distance above arbitrary electronic components. Key components of the scanning system are novel miniaturized active electro-optical time-domain ultra-wideband E- and H-field sensors for the frequency range from 0.01 to 6GHz measuring the vector field distribution with a dynamic range of 120dB. The full optical isolation of the probes eliminates disturbance of the field of the DUT compared to electrically connected probes and offers up to 60dB better sensitivity than passive electro-optical probes.

1. Introduction

Near-field radio-frequency (RF) electromagnetic field (EMF) measurements are of growing importance in various areas of research and industrial applications. Conventional near-field probes are based on diode-loaded field transducers. These probes can be designed to be very small, have minimal field perturbing properties and a wide frequency range. The RF signal pick-up of the electric (E-) or magnetic (H-) field sensor is rectified to direct current (DC) at the probe tip. While the DC output signal is proportional to the magnitude of the measured field strength, the information about the frequency and phase of the RF signal is lost. In addition, the response time of conventional probes is often limited by inherently long R-C time constants. On the other hand, traditional fast probes for electromagnetic compatibility (EMC) measurements are typically directly connected via conductive RF cables that impact on the receiving pattern and phase centre of the probe due to cable pick-up. Further, these probes considerably perturb the local field distribution at the device under test (DUT) as they are not appropriately isolated. An ideal near-field measurement tool should deliver full spectral and phase information while having minimal impact of the measured field and providing a fine spatial resolution.

2. Objectives

The aim of the presented work was the development of active electro-optical sensors for complex-valued E- and H-field vector near-field measurements in the RF domain. To serve the latest requirements in near-field EMC/EMI analysis, the goal was also to integrate our novel sensors into a fully automated μm - resolution near-field testbed.

3. Methods

The probe systems use direct laser modulation for signal transmission and electrically small transducers to pick up the E- or H-field. The system consists of a sensor head and a remote unit (Fig. 1), the concept of which have been described in [3]. Every probe contains a sensor head and a sensor identifier (ID). The sensor head is located at the very tip of the probe and contains the actual electric- or magnetic-field sensor while the sensor ID is located in the rear of the probe body. The function of the sensor ID is to uniquely identify each probe to the remote unit and to provide a redundant optical link, which is continuously monitored for LASER safety. The remote unit acts as the photonic power supply in the power-over-fiber forward link. At the sensor head the photonic energy is converted into electrical energy from which the active elements in the sensor head are supplied. The sensor head uses electrically small transducers to pick up the E- or H-fields. The RF signal from the transducer is amplified by a low noise amplifier (LNA) and modulates the optical output of a high speed VCSEL (vertical cavity surface emitting LASER). The optical signal from the VCSEL is then transmitted to the remote unit over an optical fiber. At the remote unit, the optical signal is demodulated by means of a high speed photodiode (PD), amplified by a transimpedance amplifier (TIA), and made available over a standard 50Ω output to connect a standard measurement receiver such as an oscilloscope or spectrum analyser. This sensor concept allows highly sensitive fully electrically isolated miniature near-field sensors with a large bandwidth of 10MHz

978-1-4673-5225-3/14/$31.00 ©2014 IEEE

to > 6GHz to be designed. Due to the large bandwidths with optimized flat frequency domain response, i.e., presenting a non-dispersive system for wide-band time-domain signals, we call our sensor implementations TDS (time domain sensors).

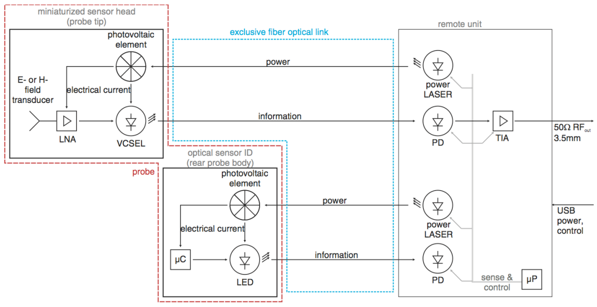

Figure 1: Schematic of the active electro-optical sensor platform consisting of a miniature sensor head that is exclusively linked via fibre optics to a remote unit

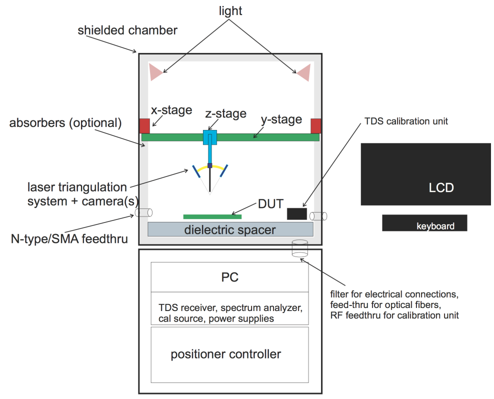

Figure 2: Schematic diagram of the novel near-field Interference and Compatibility Evaluation System (ICEy).

Fig. 2 shows the schematic of the developed near-field testbed that integrates our novel TDS probes. The ICEy (Interference and Compatibility Evaluation System) is an integrated testbed composed of a shielded, anechoic chamber where the actual near-field scans are performed, which sits on top of an equipment rack containing all necessary control and measurement equipment. The positioner system consists of linear motion stages allowing the positioning of the probe in a Cartesian coordinate system. In addition, the system allows the probe to be rolled around its axis.
The positioner system contains a LASER triangulation and camera system fixed to the z-axis that allows photographs of the device under test (DUT) to be taken as well as reconstruction of the surface profile of the DUT before the actual scans are performed. Based on the profile of the DUT, scans can be performed conforming to the surfaces of arbitrary electronic components without the need for CAD data or problematic mechanical surface detection. In the post-processing software, the photographs of the DUT can be projected onto the profile and the measured field results can be displayed as a direct overlay to the DUT.

4. Results

Based on the active electro-optical sensor platform we have developed 4 types of 1-dimensional E- and H-field sensors: a) E1TDSx: E-field sensor with sensing direction orthogonal to the probe axis; b) E1TDSz: E-field sensor with sensing direction parallel to the probe axis; c) H1TDSx: H-field sensor with sensing direction orthogonal to the probe axis; d) H1TDSz: H-field sensor with sensing direction parallel to the probe axis.

The H1TDS and E1TDS sensors were characterized in a waveguide based calibration system [1] in the frequency range from 0.01GHz to 6GHz. Fig. 3 shows the frequency response of the H1TDS and E1TDS probe system, respectively. Both probe types show a very flat frequency response over a large bandwidth. This feature allows the probes to be applied not only for frequency domain measurements, but also for wideband time domain measurements without the explicit need for correction of the dispersion due to a varying frequency domain response. The overall specifications of the TDS sensor designs are summarized in Table 1.

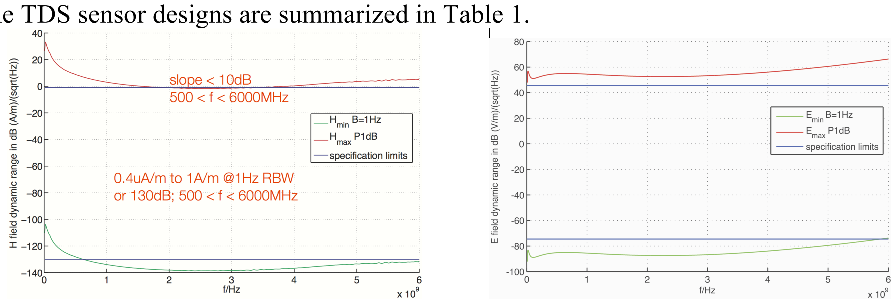

(a) H1TDSx H-field Probe (b) E1TDSx E-field Probe

Figure 3: Dynamic range upper (1dB compression point) and lower (displayed average noise floor) detection limit curve is inversely proportional to the probe sensitivity.

Fig. 4 shows the developed EMC near-field testbed prototype. Shown is the RF shielded chamber (without door) which contains the linear positioner stages. The measurement volume is surrounded by ferrite-backed flat RF absorbers (Emerson & Cuming, ECCOSORB FHY-NRL) in order to reduce reflections from the sidewalls of the shielded chamber. A dielectric spacer (made from laminated glass) is placed on top of the bottom absorber to form the measurement platform. When the DUT is placed on the glass platform, the system simulates approximately free-space conditions. Alternatively, a ground plane panel can be introduced on top of the glass platform, which introduces an additional electrically conductive boundary condition at the bottom, e.g., simulating a metallic housing below the DUT. The camera system and the LASER triangulation system are attached on the z-axis of the positioner system. This configuration provides the functionality to scan the entire measurement volume with the color camera and the LASER triangulation system. The color camera has a resolution of 0.07×0.07 mm^2/pixel. With the ability to move the camera, a coarse pre-detection of the DUT elevation profile can be performed based on the stereovision and synthetic aperture principles. The fine detection of the DUT surface structure is based on the LASER triangulation system, with the algorithms for sub-pixel LASER-line detection implemented in our system [2] reaching a resolution of better than 20µm.

TABLE I. TIME DOMAIN SENSOR SPECIFICATIONS

	H1TDSx/z	E1TDSx/z
Sensor Type	Shielded loop	Dipole
Sensor Size	4 mm^2	2.8 mm
Signal Link	Optical, for high electrical isolation	
Dynamic Range	>130 dB at 1 Hz RBW: 0.3 µA/m - 1 A/m	120 dB at 1 Hz RBW: 0.15 mV/m - 150 V/m
Parasitic E/H sensitivity	<-20 dB (at 2 GHz)	Not applicable
Frequency Range	10 MHz - 6 GHz	

TABLE II. INTERFERENCE AND COMPATIBILITY EVALUATION SYSTEM (ICEY) SPECIFICATIONS

Axis travel (x,y,z,rotation)	$500 \times 600 \times 100$ mm^3 360 degrees
Scanning volume	$500 \times 500 \times 100$ mm^3
Absolute positioning unc.	± 25 µm, 1 degree
Relative positioning unc.	±12 µm, 0.1 degree
Probe repository	4 probes, supporting automatic ex-change
DUT image acquisition	1296×966 pixels, 16 mm lens, resolution: 0.07×0.07 mm^2/pixel
DUT surface reconstruction	LASER triangulation with sub-pixel LASER line recognition De-tection limit: ±20 µm
Vector signal analyser	3.6 GHz or 14 GHz
AC power	110 - 230 V
Overall dimensions	$1.13 \times 1.13 \times 1.9$ m^3
Total mass	900 kg

On the left side of the testbed chamber, a probe repository is installed which can hold up to 4 different probes. The positioner system can exchange the probes automatically as shown in Fig. 5. This feature allows fully automated scans to be performed, even if different probe types are required for the evaluations. This is particularly handy for measurements where millions of measurement points have to be acquired, which can easily require measurement times spanning several hours. Table 2 summarizes the specification of the scanner system.

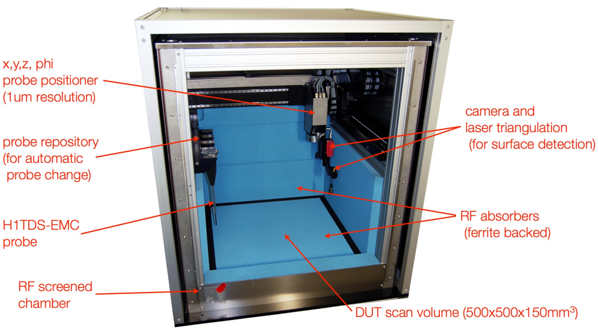

Figure 4: Photograph of the ICEy scanner. Shown is the shielded chamber (without chamber door) containing the x, y, z positioners, the probe repository with an E1TDS probe and a camera and LASER triangulation module.

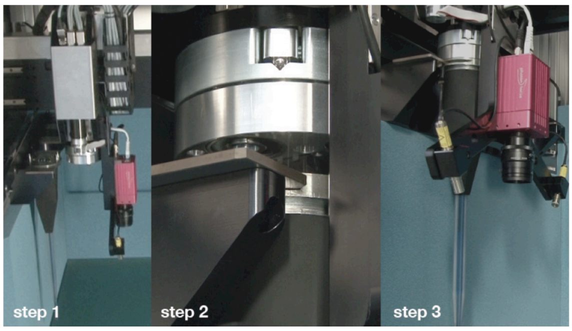

Figure 5: Automatic probe exchange process: 1) the positioner approaches the selected probe in the repository, 2) the probe head mates with the probes, 3) the positioner removes the probe from the repository.

The control software of the scanner was also designed with the aim of maximized autonomous operation requiring user interaction only at the beginning of the scan process, thus omitting operator presence during time-consuming scans. The following scan process was implemented. Step 1: The system automatically acquires the surface photographs of the DUT in tiles, combines them and displays them graphically (time <60s). Step 2: The user graphically plans the required measurements:

- Selection of scan volumes (volume size, resolution).
- Definition of measurements that are performed at every spatial point (a set of frequency or time-domain measurements).
- Definition of the quantities of interest (E-, H-Field, specific vectorial components).
- Definition of a specific probe type for specific quantities (optional).

Step 3: The system automatically acquires the DUT elevation profile and autonomously performs the defined scans. Step 4: The user can visualize the results graphically.

4.3 System Validation

Fig. 6 shows a typical validation setup and the corresponding validation results performed with the developed EMC/EMI scanner. For the validation purpose we have designed a simple microstrip line structure that can be fed and monitored with calibrated equipment externally (signal generator and power meter). This validation structure is a wide-band device with an H-field distribution above the microstrip that is known analytically. We have used this validation source to validate the performance of an H1TDSx probe within the ICEy testbed. The results illustrate the measurement accuracy of our TDS probe system and the ICEy scanner. Despite a strong field gradient in the near-field of the source our miniature field probes are able to accurately resolve the field distribution. With the completely isolated sensor design we prevent adverse loading of the source even at very close distances. In addition, it allows to design probes with an almost ideal sinusoidal receiving pattern, which is not distorted by line pick-up as in traditional EMC probes. Further, our novel probes, for the first time, allow to measure not only relative field distributions but are fully calibrated for E- or H-field measurements, i.e., allow to extract also the absolute magnitudes of the vector field components. Providing a truly calibrated field measurement, the system is the first testbed providing EMC/EMI near-field measurement results based on traceable international calibration standards and hence superior comparability between laboratories and DUTs.

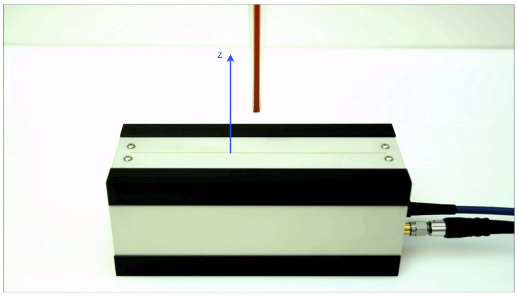

(a) Microstripline validation measurement setup.

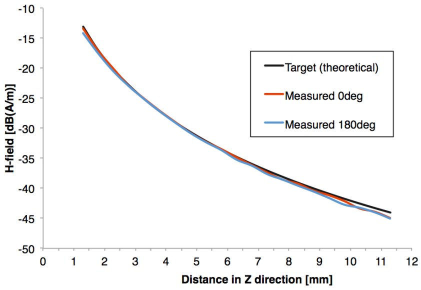

(b) Microstripline validation measurement results.

Figure 6: Microstripline H-field validation performed with the ICEy near field EMC/EMI testbed at 900MHz. Shown in b are the theoretical results of H-field decay away from the center of the microstrip and the corresponding measurement results using an H1TDSx probe. The scan was repeated with the probe rotated 180 degree to illustrate the known non-distorted receiving pattern (ideal sinusoid) of the probe.

5. Conclusion

We have developed an automated near-field testbed for system- to chip-level EMC/EMI evaluations in the RF domain. The scanning system combines a large scanning volume of $500 \times 500 \times 100$ mm^3 with micrometer resolution. A novel optical surface reconstruction system allows measurement of the surface profile of the DUT with better than 20µm uncertainty. This allows scanning at a precise distance above arbitrary electronic components. Key components of the scanning system are novel active miniaturized electro-optical time-domain E- and H-field sensors in the frequency range from 0.01 to 6GHz measuring the complex amplitude with a dynamic range of >120dB. The full electrical isolation of the probes eliminates the disturbance of the field of the DUT compared to electrically connected probes and offers up to 60dB better sensitivity than passive electro-optical probes. The applicability of our measurement system to near-field EMC/EMI scanning tasks has been successfully demonstrated. Providing a truly calibrated field measurement, the system is the first testbed providing EMC/EMI near-field measurement results based on traceable international calibration standards and hence superior comparability between laboratories and DUTs.

6. References

1. K. Pokovic, “Advanced Electromagnetic Probes for Near-Field Evaluations," Ph.D. dissertation ETH Nr. 13334, ETH Zurich, Zurich, Switzerland, 1999.

2. J. F. Collado, “New Methods for Triangulation-Based Shape Acquisition Using LASER Scanners,” Ph.D. dissertation, University of Girona, Spain, 2004.

3. A. Kramer, P. Müller, U. Lott, N. Kuster, F. Bomholt, “Electro-Optic Fiber Sensor for Amplitude and Phase Detection of Radio Frequency Electromagnetic Fields,” *Optics Letters*, **31**, July 2006, pp. 2402-2404.